HHS Public Access

Author manuscript

ACS Biomater Sci Eng. Author manuscript; available in PMC 2021 April 13.

Published in final edited form as:

ACS Biomater Sci Eng. 2020 April 13; 6(4): 2251–2262. doi:10.1021/acsbiomaterials.9b01774.

Enhancing Collagen Mineralization with Amelogenin Peptide: Towards the Restoration of Dentin

Kaushik Mukherjee[§], **Gayathri Visakan**[§], **Jin-Ho Phark**[‡], **Janet Moradian-Oldak**[§]

[§]Center for Craniofacial Molecular Biology, Division of Biomedical Sciences, Herman Ostrow School of Dentistry, University of Southern California, 2250 Alcazar Street, Los Angeles 90033, United States

[‡]Herman Ostrow School of Dentistry, 925 W 34th St., University of Southern California, Los Angeles 90089, United States

Abstract

Mammalian teeth primarily consist of two distinct calcified tissues, enamel and dentin, that are intricately integrated by a complex and critical structure, the dentin-enamel junction (DEJ). Loss of enamel exposes the underlying dentin, increasing the risk of several irreversible dental diseases. This paper highlights the significance of utilizing the functional domains of a major enamel matrix protein, amelogenin, intrinsic to tooth enamel and the DEJ interface, to rationally design smaller bioinspired peptides for regeneration of tooth microstructures. Using this strategy, we designed a synthetic peptide, P26, that demonstrates a remarkable dual mineralization potential to restore incipient enamel decay and mineralization defects localized in peripheral dentin below the DEJ. As a proof of principle, we demonstrate that interaction between P26 and collagen prompts peptide self-assembly, followed by mineralization of collagen fibrils *in vitro*. P26-mediated nucleation of hydroxyapatite (HAP) crystals on demineralized dentin *in situ* significantly facilitates the recovery of mineral density and effectively restores the biomechanical properties of dentin to near-native levels, suggesting that P26-based therapy has promising applications for treating diverse mineralized tissue defects in the tooth.

Graphical Abstract

Corresponding Author: joldak@usc.edu (J. M-O).

Supporting Information

Binding affinity of P26 with HAP, tensile strength testing sample preparation schematic.

Conflict of Interest

The authors declare no conflict of interest.

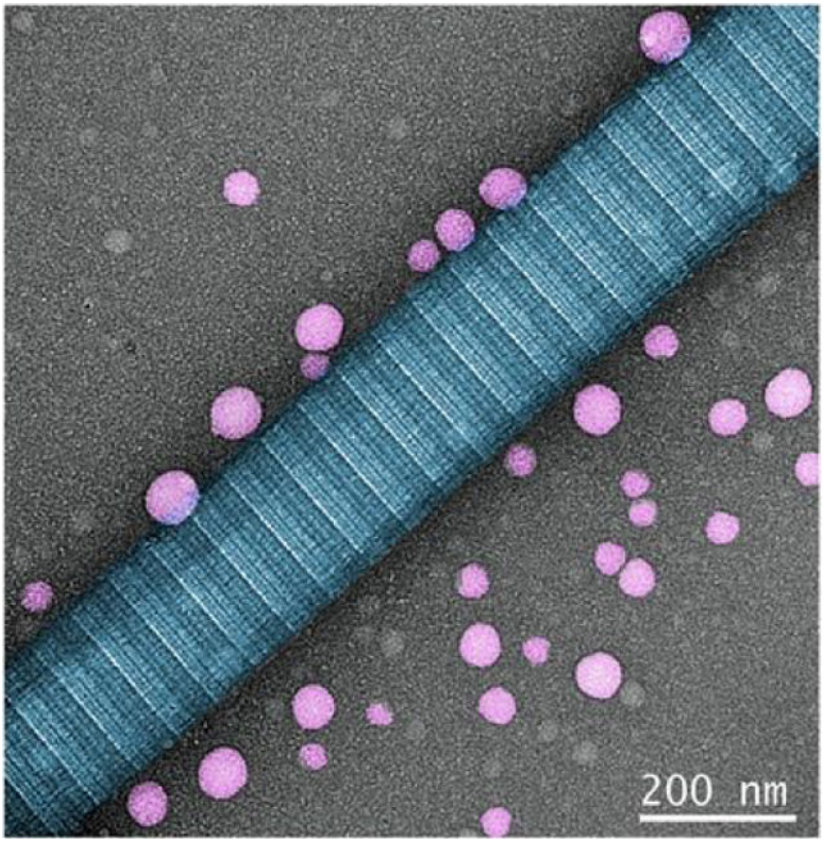

Peptide assembles as spherical nanoparticles aligned closely along the collagen fibrils *in vitro*

Amelogenin is a prime candidate for the design of bioinspired, self-assembling peptide (P26) with a distinctive dual biomimetic remineralization in enamel and dentin. P26 assembled into discrete nanoparticles along collagen fibrils to promote functional remineralization in dentin lesions. Densely- packed HAP crystals occluded the open tubules, sheathed the exposed collagen fibrils and enhanced mineral recovery to restore the biological and biomechanical properties of demineralized dentin.

Keywords

dentin; enamel; biomimetics; remineralization; amelogenin peptide; collagen

1. INTRODUCTION

The biological formation of nanocomposites in mineralized dental tissues such as enamel and dentin rely on a coordinated series of highly complex macromolecular, cellular and matrix-mineral interactions that are particularly challenging to mimic. Understanding the fundamental principles of biomineralization and the organo-mineral spatial interactions at their interfaces can therefore offer valuable insights into designing bioinspired materials for the restoration of damaged dental tissues.

The structure of the mammalian tooth is designed to provide a certain damage tolerance.[1] In enamel, this is achieved by the hierarchical architectural design of hydroxyapatite (HAP) crystals (30 nm thick and 60 nm wide) exhibiting a preferred c-axial orientation, packed within rods (4–8 μm diameter) that are separated by interrod structures.[2] This confers biological advantages of extreme hardness and wear resistance to the tooth. On the other hand, the brittleness of enamel requires the presence of underlying dentin to dissipate and transmit the occlusal forces. Structurally, dentin is permeated by arrays of small, parallel dentinal tubules (~1 μm diameter peripherally) in a mineralized collagenous matrix.[3] It constitutes the bulk of the mineralized tissue in the tooth and is vital for the tooth's overall high-compression elastic modulus, shear modulus and tensile strength. The vital interface between the two distinct calcified tissues, the dentin-enamel junction (DEJ), provides a crack-arrest barrier mechanism that diminishes stress concentration at the crack tip,[4,5] thereby contributing to the fracture toughness of dentin.

In humans, damage to the exterior layer of protective enamel can occur either through the development of carious lesions or through non-carious cervical lesions (NCCLs) due to attrition, abrasion, abfraction or dental erosion. These processes expose the dentin at the DEJ, jeopardizing the integrity of the tooth and the inner vascularized dentin-pulp complex. Successful restoration of NCCLs is becoming an increasingly important determinant of the long-term health of the tooth. Such lesions are invariably affected by their location, the nature of occlusal loading, and tensile or compressive stress distribution patterns, which are reflected particularly in the cervical areas of the tooth.[6,7]

While the biological and functional design principles of dental tissues enable them to respond to complex stresses as a single unit, traditionally enamel[8–16] and dentin[17–19] have been addressed as separate entities in attempts at their biomimetics. An important novelty of the present study thus lies in rationally designing a single bioinspired peptide with dual biomimetic mineralization potential for enamel and dentin repair. Harnessing of peptides designed in this manner have the potential to restore incipient enamel decay, reinforcing the tooth against loss of mineral density, tensile strength and mechanical properties as it restores the circumpulpal dentin near to its native state.

The selection of the major enamel matrix protein; amelogenin, as an archetype for biomineralization has been well established through several *in vitro*[20,21] and animal studies.[22–26] Amelogenin in enamel and non-collagenous matrix proteins (NCPs) in dentin influence the organization and growth of HAP crystals during the biomineralization processes. Proteomic analysis of the DEJ interface in human molars has revealed high biological activity, predominantly rich in collagen (Type I) and enamel-specific proteins such as amelogenin and ameloblastin.[27,28] Hence, interactions between amelogenin and collagen fibrils at the DEJ reinforce the functional continuity of the 3D hierarchical micro-scalloped interface. Recent studies have indicated that collagen fibrils guide the assembly of amelogenin into organized linear chains and that interactions between the two major extracellular matrix proteins direct oriented mineral growth, prompting collagen mineralization.[29] The close interactions between these two major macromolecules therefore deserve attention for their potential applications in dental hard tissue regeneration.

Successful repair of demineralized dentin requires a complete spatial and hierarchical relationship between mineral ions, collagen scaffold and the organic NCPs to effectively induce inter- and intrafibrillar collagen mineralization.[30] Diverse strategies have been implemented to promote surface remineralization of dentin, including fluoride-based products,[31] amorphous calcium-phosphate (ACP)-releasing resins[32] and bioactive glasses.[33,34] However, these approaches have failed to promote the mineralization of exposed collagen fibrils, as seen in intact dentin, which is vital to restoring the biomechanical properties of the tissue. Innovative remineralization systems have been employed to mimic the activity of the NCPs in promoting collagen mineralization, such as polymers (PILP),[35,36] biomimetic analogs[37–39], polyelectrolyte-directed mineralization[40], agarose gels[41,42]and dendrimers.[43,44]

We have recently shown that an amelogenin peptide P26 [12] includes the apatite-binding and self-assembly regions, important functional domains that promote the regrowth of multi-layered oriented HAP nanostructures on the surface of demineralized enamel, integrating them with the underlying tissue and enhancing mechanical function[10]. Here, we demonstrate that P26 is uniquely suited for dual enamel-dentin remineralization and repair while co-assembling with collagen fibrils. The aims of this study were to repair superficial dentin below the DEJ using P26 and to examine numerous facets of dentin biomineralization through *in vitro, in situ* and functional studies.

We implemented a new generation of peptide-mediated biological strategy for the restoration of superficial dentin by a) promoting collagen mineralization, b) reinforcing HAP mineral density in demineralized dentin, c) increasing tensile strength and d) restoring dentin hardness and modulus to withstand functional challenges in the oral cavity.

2. MATERIALS AND METHODS

2.1. Peptide synthesis.

Peptides P26 [12] and Leucine-Rich Amelogenin Peptide (LRAP)[11] were synthesized commercially at ~95.13% purity (CHEMPEPTIDE Limited). Both peptides were phosphorylated at the N-terminal Ser which is equivalent to the Ser16 on full-length amelogenin. High-performance liquid chromatography and mass spectrometry were used for peptide purification and mass determination by the company prior to shipment. For sequences of P26 and LRAP see references 11 and 12.

2.2. Characterization of secondary structures by circular dichroism.

Samples of P26 (0.2 mg/ mL), Type I collagen (1 mg/mL) and P26-collagen mix were dissolved in HEPES buffer (10mM) t pH 7.15 and incubated for 30 min at RT. Circular Dichroism (CD) spectra were collected in high-transparency quartz cuvettes (250 μL) with a path length of 1 mm and band width of 2 nm at 25 °C in the far UV spectral range (190–260 nm) using a JASCO J-815 circular dichroic spectrometer. Conformational changes in the secondary structure of the peptide induced by collagen were investigated at physiological pH by subtracting the spectra of collagen alone.[45] All the CD spectra collected were normalized to mean residual ellipticity (MRE) values.

2.3. Collagen self-assembly.

Purified Type I collagen solution (3 mg/mL) (Gibco, Life Technologies) from rat tendon dissolved in 0.1 M acetic acid (pH 3) was kept at 4 °C. A final concentration of 1 mg/ mL collagen was obtained in 1X PBS buffer (pH 7.8) in 100 μL solution. The initial pH recorded was ~5.5–6 and was gradually increased to pH 7 by adding 100 mM NaOH in small increments (0.5–1 μL). A droplet (30 μL) of this solution was placed on an inert polyethylene substrate in a closed chamber and a 400-mesh carbon coated Transmission Electron Microscopy (TEM) grid (Ted Pella, Inc.) was placed on top of the droplet. The solution was incubated for 3 h at room temperature (RT). After the incubation, the collagen-coated grids were taken out of the chamber, washed with double distilled water (DDW), blotted with a filter paper and air-dried. To analyze self-assembled collagen fibers under TEM (100 kV, JEOL 4500), the grids were stained with 2% uranyl acetate solution for 5 min, washed and air-dried again.

2.4. Self-assembly of peptide (P26) in the presence of collagen.

Peptide P26 (0.2 mg/mL) was dissolved in DDW and the pH adjusted to 7.2 using NaOH solution according to a previous protocol.[14] Following the protocol for imaging self-assembly of collagen fibrils,[44] a droplet of the peptide solution was placed on an inert polyethylene substrate in a closed chamber and the collagen coated TEM grid (unstained) was placed on top of this droplet. The sample was incubated for 3 h at RT in a closed chamber, rinsed, blotted, air-dried and stained with 2% uranyl acetate solution for 5 min for TEM analysis.

2.5. Collagen-P26 mediated apatite mineralization in vitro.

A mineralizing solution was prepared with and without peptide to get a final concentration adjusted to pH 7 in DDW (1.67 mM $CaCl_2.2H_2O$, 1 mM Na_2HPO_4, 1.25 mM NaOH and 0.2 mg /mL P26, respectively).[29] Droplets of the mineralization solution (30 μL) were placed in the humidity chamber and the collagen-coated carbon grids were placed on top and incubated for 1 h and 2.5 h. After incubation, the TEM grids were washed with deionized water, air-dried and characterized by TEM (200 kV, JEOL 4500). Selected-Area Electron Diffraction (SAED) of the mineralized collagen fibrils was performed to identify the presence of mineral phases at 30000x magnification. For each group (with and without P26), 3 TEM grids were analyzed.

2.6. Remineralization of demineralized dentin discs with and without P26.

Caries-free human third molars extracted using standard procedures (Herman Ostrow School of Dentistry, USC) were used in this study. Remnant soft tissues were removed using a scalpel and the teeth were rinsed in 70% ethanol to get rid of gross debris. Molars were sectioned transversally into 2 mm thick discs at the mid-coronal region of the tooth. A window of sound dentin measuring 2 × 2 mm was delineated by applying two coats of acid-resistant nail varnish on the tooth surfaces. To mimic carious lesions, the samples were immersed in a demineralizing solution buffer (2 mM $CaCl_2{\cdot}2H_2O$, 2 mM KH_2PO_4, 50 mM sodium acetate, and 0.05 M acetic acid) at pH 4.6 for 3 days at 37 °C.

Demineralized dentin discs were dried, divided into P26 treated and control groups (n=6 each), and placed in clean glass vials. Dentin discs for the P26-treated group were immersed in 100 μL (0.5 mg/mL) of P26 solution and were left undisturbed at RT overnight. All the discs were then placed in 5 mL of artificial saliva solution (1.2 mM $CaCl_2{\cdot}2H_2O$, 50 mM HEPES buffer, 0.72 mM KH_2PO_4, 16 mM KCl, 4.5 mM NH_4Cl, 0.2 mM $MgCl_2{\cdot}6H_20$, and 1 ppm NaF) at pH 7.0 and incubated in a water bath at 37 ˚C for 10 days. Artificial saliva solution was changed every 24 h to prevent the chance of potential contamination and to replenish the ions in the solution. Peptide was re-applied on the samples in the P26-treated group on Day 5 of the remineralization cycle. Control discs were remineralized in artificial saliva without any pretreatment with peptide.

2.7. Nano-SEM sample preparation for dentin discs.

Remineralized dentin discs were prepared for SEM analysis to study the morphology, composition and location of the CaP precipitates. To preserve the surface details of dentin specimens and prevent the collapse of collagen fibrils, the dentin discs were dehydrated with increasing concentrations of ethanol (10–100% in 10% increments), chemically dried using HMDS (hexamethyldisilazane) and sputter-coated with a Platinum Palladium mixture at a weight% ratio of 80/20 for 45 s to be viewed under Field Emission Scanning Electron Microscopy (FESEM, FEI Nova Nano SEM 450). Element analysis and mineral content was determined using an energy-dispersive X-ray microanalysis detector coupled to the SEM (JEOL 7001 SEM-EDX). A 360 μm^2 area was analyzed from each disc with an acquisition time of 200 s at 10 kV (n=3).

2.8. Evaluation of gain in mineral density of partially demineralized dentin after P26 treatment using micro-CT (μ-CT).

Molar teeth were sectioned as 1.2 ± 0.2 mm thick dentin discs obtained 1.5mm above the Cemento-Enamel Junction (CEJ). Hydrated dentin discs were randomly divided into two groups: P26-treated and control (n=10). Mineralization experiments were performed as described in section 2.6. Micro-CT system was calibrated using 250 g/cm^3 and 750 g/cm^3 HAP phantoms (Micro Photonics Allentown, PA, USA) against the attenuation coefficient of the phantoms. A μ-CT scanner (SkyScan 1174 μ-CT, Micro Photonics Allentown, PA, USA) operating at 52 kV, 790 mA, 0.5 mm aluminum beam filter was used. A voxel size resolution of 9.6 μm was selected following optimization experiments that were conducted at varying resolutions in order to achieve the lowest noise to signal ratio. Each dentin disc (from both groups) was scanned thrice corresponding to normal, demineralized and remineralized dentin. The projection dataset obtained through 3D reconstruction using NRecon (software, version 1.6.9.8; SkyScan Bruker) was viewed on Amira 6.5.0 (Thermo Fisher Scientific). Representative samples were selected to obtain images of normal, demineralized, P26-treated and control dentin. 3D reconstructed images were sectioned axially and viewed using the heatmap setting. The projection dataset was then further analyzed using CTAn (Software Version 1.6.9.8; SkyScan Bruker) to record quantitative measurements of Bone Mineral Density (BMD or MD). Paired sample t-tests were carried out in Microsoft Excel between demineralized dentin MD and remineralized dentin MD in both the P26-treated and control groups. The significance level was set at 0.05.

2.9. Evaluation of increase in tensile strength in dentin after P26 treatment.

Transverse dentin sections (0.7 ± 0.2 mm thickness, and 1.4 mm above the CEJ) were obtained using a low-speed diamond saw under constant water cooling (BUEHLER IsoMet 1000) (Figure S2a, b, Supporting Information). Transverse sections were further prepared into hour-glass shaped test specimens using a dental handpiece ensuring copious irrigation. For each sample, an effective test site area of 1 mm^2 was chosen. Tensile strength test specimens were then divided into 4 groups: normal dentin, demineralized dentin, P26-treated demineralized dentin, and control (n=~10–15 per group). All the surfaces other than the test site area were covered with two coats of acid resistant nail varnish. Demineralization and remineralization of the test specimens were carried out as described in section 2.6. Prior to tensile strength testing, varnish coating on the samples was carefully mechanically removed and the samples were immobilized on the grips of a Ciucchi's jig (Figure S2c, Supporting Information) using cyanoacrylate glue (Scotch, USA). Hydrated test specimens were then tested under tension using a Universal Testing Machine (Instron 5965 operating at 0.5 mm/min) until fracture. The maximum load calculated by the machine in Newtons (N) was then converted to tensile strength in megapascals (MPa) by calculating the force/unit cross-sectional area at the test site. Data were gathered only from those test specimens that fractured in the desired test site. Statistical tests were carried out either in Microsoft Excel 2018 (parametric tests) or using online calculators (non-parametric tests).

2.10. Mechanical properties of remineralized dentin.

Nano-indentation was used to determine the elastic modulus and nano-hardness of the dentin discs treated with the peptide compared with those of the control. Four different groups (healthy dentin, demineralized dentin, control and P26 -treated dentin) were measured (p 0.05; n=3). Berkovich diamond indentation tip was used to make 25 indentations on each tooth sample. A continuous stiffness measurement (CSM) was used to measure the hardness (strength) and the elastic modulus (stiffness) at a constant strain rate of 0.05 $s^{-1}$and measuring depth up to 2 μm. The distance between the indentations was maintained at 50 μm to prevent interference of residual stresses from adjacent indents. Fused silica was used as the standard calibration material. All the statistical analyses were carried out using software (Origin 8.0, Origin Lab, Northampton, MA and Microsoft Office Excel 2007).

3. RESULTS

3.1. P26 interacts with collagen fibrils *in vitro* and promotes mineralization.

Circular dichroism spectroscopy (CD) was used to investigate conformational changes in P26 with the addition of collagen at physiological pH (Figure 1a, b). At pH 7.15, the collagen (1 mg/ mL in HEPES buffer) showed a strong minimum negative peak at 208 nm and a strong positive maximum at 226 nm at 25 °C, which are characteristic of a triple helical protein conformation.[46] P26 displayed a characteristic random-coil conformation with a sharp negative ellipticity with a minimum at 200 nm.

Upon addition of collagen (1 mg/ mL) to P26 (0.2 mg/ mL), the negative minimum peak shifted left to 198 nm with a weak positive maximum at 227 nm (Figure 1a). The data was normalized[45] and subtracted from collagen background alone, and the structural changes to

P26 induced by collagen revealed a significant decrease in the negative peak intensity and a shift to the left of the spectrum to 198 nm, implying collagen induced changes in the secondary structure of the peptide upon interaction (Figure 1b). The low amplitude in P26 after incubating with collagen may be due to peptide assembly with the collagen fibrils, reducing the spectrum of the peptide.

Building on these findings, the self-assembly of collagen fibrils was carried out at room temperature (RT) and pH 7 on the surface of 400-mesh TEM grids. TEM analysis of negatively-stained Type I collagen fibrils revealed a characteristic 67 nm axial periodicity (D-period) and “gap– overlap” structure (Figure 1c, d). The fibrils had a diameter of ~185 nm. Peptide assembly experiments in the presence of collagen fibrils resulted in distinct homogenous spherical particles distributed densely on the surface of the TEM grid (Figure 1e, f). Peptide assemblies associated with collagen fibrils were seen as linearly dispersed nanospheres, either isolated or in aggregates, aligned closely along the surface of collagen fibrils (Figure 1f). The majority of the spherical assemblies fell into one of two groups: those with a diameter of 27±4.9 nm and those with a diameter of 50±15.2 nm.

To investigate peptide-mediated collagen mineralization events, the collagen fibrils were incubated with or without P26 in metastable calcium phosphate solution for different time intervals. After 1 h, the control samples (without P26) showed very few randomly distributed mineral deposits around the collagen fibrils on the TEM grid surface (Figure 2a, b). In contrast, after 1h of mineralization in the presence of P26 (0.2 mg/mL) (Figure 2c, d), swollen collagen fibrils with apparent increased diameter were seen suggesting ACP nanoparticle infiltration.[47] As shown by the yellow arrows in Figure 2d a few amorphous minerals lying on or in close proximity to collagen fibrils were also observed.

After 2.5 h of mineralization, the control sample (Figure 3a, b) showed a slight increase in mineral density on the collagen fibrils but the mineral particles were too large to penetrate the fibrils (Figure 3b). Progression of collagen mineralization in the presence of P26 (Figure 3c, d) gradually transformed collagen’s structure into smooth, electron-dense fibrils with SAED showing arcs characteristic to HAP (inset in Figure 3d). The multitude of mineralizing specks seen after 1 h of incubation with P26 gradually transformed to ribbon-like forming crystals (red arrow) scattered densely in the background (Figure 3d), suggesting acceleration of HAP nucleation by P26. There was also evidence of extrafibrillar mineralization on the surface of collagen fibrils, as shown by the larger apatitic mineral deposits (yellow arrows) aligned closely on the fibril surface.

3.2. P26 promotes remineralization of dentin discs *in situ*.

To study P26-mediated remineralization of dentin *in situ*, we carefully sectioned sound human molars bucco-lingually in the mid-coronal region just below the DEJ in the upper one-third of the circumpulpal dentin. Normal dentin had tubular structure surrounded by a cuff of hyper-mineralized peritubular dentin. Intertubular dentin, being less mineral-dense, appeared dull in comparison. Following graded ethanol dehydration and chemical fixation, the collagen networks in the dentin specimens were apparent (Figure 4).

After 3 days of demineralization at pH 4.6 and at 37 °C, the surface appearance of sound dentinal tubules (1–1.5 μm diameter) was significantly altered. The dentinal tubules widened to nearly twice their normal diameter (~3 μm diameter) and the distinction between peritubular and intertubular dentin was lost (Figure 4a, b). The zone of dentin demineralization spanned a depth of approximately 50–80 μm and the partially demineralized collagen fibrils appeared smooth and devoid of minerals (Figure 4b). SEM images of the control dentin discs (without P26) after 10 days showed no discernible changes in tubule diameter or collagen architecture and remained similar in appearance to demineralized dentin. The tubules remained open with no evidence of remineralization on the surface of the collagen fibrils (Figure 4c, d). In contrast, dentin discs treated in P26 for 10 days remineralized, showing a dense HAP coating occluding the open-tubules on the surface and around the periphery of the tubules (yellow arrows) (Figure 4e–h). Application of P26 peptide also led to the deposition of multiple electron-dense mineral deposits in the intertubular dentin matrix over the collagen fibers, indicative of collagen mineralization (red arrows shown in Figure 4f).

Carious attack can lead to tooth surface loss and subsequent exposure of the dentin organic matrix, causing degradation of the collagen fibrils. Cross-sectional evaluation of control dentin specimens (remineralized with artificial saliva) (Figure 5a, b) revealed mineral-depleted collagen fibrils inside the exposed dentinal tubules (red arrows in Figure 5b). In contrast to the control, P26-treated dentin (Figure 5c, d) revealed remineralization of the exposed collagen fibrils inside the dentinal tubules with a distinct ‘string of beads’ appearance of the collagen fibrils (red arrows in Figure 5d) suggestive of intrafibrillar collagen mineralization. These data corroborated with our observation of the *in vitro* experiments. Regrowth of several needle-like HAP crystals could be seen around the periphery of the tubules (yellow arrows in Figure 5d) that contributed to the restoration of the mineral density of demineralized dentin.

XRD spectra of newly deposited mineral crystals on the remineralized discs displayed sharp peaks at 2θ= 25.9° (002), 31.8° (211), 32.8° (300) and 39.8° (310) (Figure 5e),[48] consistent with the peaks of HAP. Distinct diffraction peaks at approximately 2θ= 31.8°–32.8° could be identified in the spectra, signifying good crystallinity of HAP in the peptide-mediated mineralized dentin discs. A 10 min sonication of the dentin discs indicated a well-sealed intact HAP coating firmly adherent to the occluded tubules. These peaks were not identifiable in the untreated control dentin specimens, consistent with the SEM data showing a lack of newly formed crystals at the end of the mineralization cycle. EDX analysis showed similarities in the elemental composition of normal and peptide-treated dentin (Figure 5f). The ratios of calcium to phosphate (by weight) in normal, demineralized and P26-treated dentin were 1.90±0.03, 1.57±0.05 and 1.87±0.014 respectively (n=3). Higher variability of elemental composition in acid-treated discs could be due to non-uniform demineralization across the various dentin samples.

3.3. P26 promotes gain in mineral density of treated dentin.

Micro-CT was used for the evaluation of quantitative gain in mineral density (MD) through the determination of the BMD following P26 treatment of partially demineralized dentin (Figure 6).

Following 10 days of remineralization in artificial saliva, samples in the control group did not record any statistically significant increase in MD (p= 0.1010; n=7). The mean MD after demineralization (1.08±0.18 g/cm^3) remained unchanged when remineralization was carried out without the peptide (Figure 6a–c).

The mean mineral density (MD) of hydrated, sound dentin in the P26-treated group at the beginning of the experiment was 1.52±0.06 g/cm^3 (n=10) and it declined to 1.05±0.13 g/cm^3 following 3 days of acid-mediated demineralization. In contrast to the control, all P26-treated samples recorded a MD gain ranging between 6.83%−14.43% (Figure 6d–f) Statistical analysis with paired sample t test revealed that the MD gain after P26 treatment was statistically significant ($p < 0.001$; n=10). The mean MD at the end of 10 days of remineralization with P26 was 1.16±0.13 g/cm^3.

3.4. P26 promotes increase in tensile strength of treated dentin.

As shown in Figure 7a, the mean tensile strength (TS) values of sound (64.61±13.26 MPa; n=15) dentin pulled perpendicular to the long axis of tubules were consistent with the results reported in the literature.[49] There was a 76% drop in TS of dentin following 3 days of acid demineralization, reducing the average value to 15.50±6.90 MPa (n=10). Following 10 days of remineralization in artificial saliva (AS), a partial recovery of TS to 34.40±19.94 (n=10) was observed only in the P26-treated samples .Statistical analysis using Student's t-test indicated that the difference in TS values between demineralized and P26-treated dentin samples was significant (p=0.0163).The control samples (n=10), which were remineralized in AS only, did not show any statistically significant change in TS (p=0.5179) when compared to demineralized dentin.

3.5. P26 promotes an increase in hardness and modulus of repaired superficial dentin.

Restoration of hardness and modulus was calculated using nanoindentations on the surfaces of hydrated dentin specimens to record actual loss of stiffness and nanohardness (Figure 7b, c). The modulus and hardness for sound dentin were 20.8±5.08 GPa and 0.65±0.2 GPa respectively (n=3). After 3 days of demineralization in acidic buffer (pH 4.6), the modulus and hardness of dentin reduced to 6.5±2.97 GPa and 0.27±0.13 GPa respectively, representing a ~69% decrease in modulus and 58% decrease in the hardness of the demineralized specimens (n=3). Following 10 days of remineralization, no significant increase was observed in the control samples ($p > 0.5$). On the other hand, when the demineralized samples were treated with P26 (0.5 mg/ mL) overnight, the average elastic modulus and hardness increased substantially ($p < 0.01$) to 22.5±8.6 GPa and 0.65±0.30 GPa respectively as confirmed by Student's t test. Variability in the mechanical properties of repaired dentin was minor and could potentially be due to the intrinsic variability in the mineral composition of dentin

4. DISCUSSION

We report that the amelogenin-inspired peptide P26 not only promotes biomimetic growth of enamel *in situ*[12] but is also effective in promoting collagen mineralization *in vitro* and dentin remineralization *in situ*. Our present findings have potential clinical significance in dentistry for the repair of lesions where both enamel and dentin are affected (i.e. non-carious cervical lesions). Application of short peptides has practical, financial and clinical advantages over the use of full-length protein to engineer specific material properties.

The robust interface between dentin and enamel (DEJ) is critical to preventing the shearing of tooth enamel during everyday functions like mastication. Dentin formation precedes enamel formation and is first indicated by the appearance of distinct, large-diameter collagen fibrils (0.1–0.2 μm diameter) called Von-Korff's fibrils that fan out just below the inner enamel epithelium. Interestingly, the type I collagen fibrils in mantle dentin and the incipient enamel crystals at the DEJ share a similar crystallographic orientation. This correlation has been substantiated by animal model studies in which knocking out enamel[50] and dentinal matrix proteins[51] resulted in the delamination of enamel and defects in the mineralization events at the DEJ.

This multifaceted communication between the two tissues has inspired the biomimetic design of synthetic materials to restore lost tooth structure. In this study we designed a series of experiments to interrogate the interaction of collagen fibrils with synthetic amelogenin peptide (P26) assemblies leading up to the bioinspired repair of outer demineralized dentin on an *in situ* tooth model. As revealed through the CD and TEM data analysis, the close proximity and arrangement of distinct spherical assemblies of P26 along the collagen fibril axis is indicative of interaction between the two. This may specifically be based on structural recognition by P26 of collagen triple helices, or weak molecular interactions such as electrostatic interactions between the two macromolecules. For example, P26 is an acidic phosphorylated peptide rich in negatively charged residues, namely aspartic acid (Asp) and glutamic acid (Glu), which could potentially interact with the positively charged sites on the collagen surface.[52] Previous studies have shown that collagen fibrils can facilitate the assembly of full-length amelogenin into nanospheres, similar to our findings with P26, along with fused filamentous amelogenin assemblies.[29]

It is widely acknowledged that collagen alone cannot mineralize and it utilizes highly phosphorylated NCPs, such as dentin phosphophoryn (p-DPP) and dentin matrix protein 1 (p-DMP1), to promote the infiltration of stabilized amorphous minerals into collagen compartments.[30] Further studies have provided insight into the size exclusion characteristics of type I collagen wherein molecules, peptides smaller than a 6 kDa and amorphous calcium-phosphate particles could freely diffuse into the water-filled collagen compartments to initiate nucleation of HAP crystals.[53] This would imply that mineralization in collagenous tissues like dentin and bone can be mediated through more than one mechanism, via the role of NCPs, precursor mineral phases, size exclusion, polyelectrolyte- directed mineralization systems.[30,40,54,55]

In the case of P26-collagen mediated remineralization, it is likely that the hydrophilic phosphorylated P26 (~3.14 kDa) promoted nucleation of small homogeneously sized apatite crystallites[12] in the gap and overlap regions of adjacent fibrils. Depending on the P26-mediated size of the crystallites, they would either migrate into the intrafibrillar spaces or aggregate on the surfaces.[56] Another proposed mechanism of P26-collagen-mediated mineralization could be elucidated by the small size of the peptide monomers (< 6 kDa), which allow the molecules to readily diffuse into the water-filled compartments of collagen fibrils. Here, P26 monomers could act as a sequestration biomimetic analogue (i.e. NCP's) due to a highly charged C-terminus capable of actively recruiting calcium ions and promoting apatite nucleation.[57] The high affinity to calcium and apatite crystals is supported in the present HAP binding experiments (Figure S1, Supporting Information).

Demineralization of dentin in the oral cavity at pH less than 5 could activate the MMPs and cysteine cathepsins in the dentin matrix, leading to denaturation of the collagen fibers and extracellular matrix degradation.[58] Repair of exposed dentin poses a more complex challenge than enamel remineralization due to the lack of residual mineral crystals and apatite seed crystals, which act as nucleation templates, in a mineral-depleted collagenous matrix. One of the most essential parameters determining the role of non-collagenous proteins in mineralization is to bind to specific components of collagen, accrue calcium ions in the vicinity,[59] and 'fossilize' the activated MMPs within the dentin matrix, thereby bringing down their proteolytic activity. Biomimetic analogues such as P26 could be used effectively to promote nucleation over the remnant apatite seeds to enhance dentin remineralization.

Repeated application of P26 on the surface of demineralized dentin resulted in the formation of small HAP crystals that grew around the walls of the dentinal tubules and gradually occluded the tubules (Figures 4, 5). The small size of the peptide allowed it to penetrate dentinal tubules to dynamically promote apatite crystallization, resulting in the occlusion of the open tubules. Mineralization of dentinal tubules is clinically significant in the context of addressing dentin hypersensitivity as it blocks access to the exposed nerves. This can help alleviate clinical symptoms of tooth hypersensitivity. Collectively, the SEM and XRD results also suggested that P26 can be versatile in controlling the deposition and orientation of mineral deposits on different HAP-containing tissues (enamel and dentin). Effective infiltration of HAP along the surface of the collagen fibrils was marked by the "beaded" or "swollen" appearance of remineralized collagen fibers as seen on the dentin discs. The observed gain in mineral density and mechanical function of P26-treated dentin was confirmed in parallel functional studies.

The collagen fibrils in dentin experience tensile residual strain/stress as they act as tensed strings during masticatory forces, while the embedded HAP minerals in mineralized collagen function as compression fillers that stiffen the fibers.[60] Ultimate Tensile Strength (UTS) tests of mineralized, demineralized and carious dentin have established that collagen matrix and mineral phases (around and within the collagen fibrils) contribute to the total strength of dentin.[49] While we confirmed surface collagen fibril mineralization through *in vitro* and *in situ* experiments, it would take additional experiments to give direct evidence of its mechanism. Interfibrillar mineral concentration[36] and intrafibrillar collagen

mineralization[61] are two important indicators of improved mechanical function in collagen-rich mineralized tissues, with the latter playing a critical role in increasing the elastic stiffness of demineralized dentin. In this study, supporting UTS and μ-CT data on normal, demineralized and treated dentin discs were indicative of enhanced mineral density and mineral-reinforced collagen fibers after peptide application. The important role of P26 in promoting dentin remineralization was determined by increased mineral density and micromechanical behavior as evidenced by a 2.22-fold increase in the tensile strength (34.40 MPa; $p < 0.05$), a significant gain in MD (1.16±0.13 g/cm^3; $p < 0.001$), and effective restoration of hardness and modulus of the tissue to near native levels, with an overall reduction in the demineralized lesion depth. Such notable biological and functional recovery suggests the strong potential of amelogenin-inspired biomimetic mineralizing strategies for application in restorative dentistry in cases where the repair of dentin and enamel are needed simultaneously.

5. CONCLUSION

Close communication between enamel matrix protein amelogenin and collagen at the dentin-enamel interface is critical to preserve the continuity of this vital junction. Hence, amelogenin serves as a model protein to design smaller bio-peptides that can mimic such close interactions for the repair of peripheral dentin. The present study explored the potential of using amelogenin-peptide P26 that is uniquely suited for the remineralization of enamel and dentin tissue defects simultaneously. P26 peptide mediated organized HAP crystal growth and facilitated collagen mineralization which in turn led to a significant gain in mineral density of demineralized dentin, resulting in repaired dentin with improved biomechanical properties. Whether the principal mechanism of P26 in promoting collagen mineralization is size exclusion criteria, controlled apatitic growth, combination of both or an alternative mechanism, remains to be determined. Ultimately, a systematic examination of the multidimensional interactions between organic macromolecules and mineral ions at the DEJ can provide a valuable foundation for the development of improved synthetic biomaterials associated with functionality.

Supplementary Material

Refer to Web version on PubMed Central for supplementary material.

ACKNOWLEDGEMENTS

This work was supported by grants from the National Institute of Health- National Institute of Dental and Craniofacial Research (R01, DE-13414, R21 DE-027529 and R01 DE-027632 to JM-O). The authors acknowledge Dr. Steven Nutt from the Mork Family Department of Chemical Engineering and Materials Science, Viterbi School of Engineering, University of Southern California for providing access to the Nanoindentation instrument, Anna Kallistova' for analyzing and interpreting peptide binding to HAP, Tach-Vu Ho for his assistance in Micro-CT training, and Natalie Kegulian for her help with interpreting the CD data. J.M-O. and K.M. conceived the idea, designed the experiments and analyzed the data. G.V. performed the Micro-CT analysis, tensile strength experiments and assisted in SEM-EDX imaging and analysis. J-H.P. assisted in training, analysis and interpretation of the tensile strength data using Instron 5965. J.M-O. supervised the entire project and K.M. and J.M-O wrote the manuscript. All the authors read the manuscript, commented on it, and approved its content.

References:

1. Chai H; Lee JJW; Constantino PJ; Lucas PW; Lawn BR, Remarkable resilience of teeth. P. Natl. Acad. Sci. USA 2009, 106 (18), 7289–7293. DOI: 10.1073/pnas.0902466106.
2. Daculsi G; Kerebel B, High-resolution electron microscope study of human enamel crystallites: size, shape, and growth. J. Ultrastruct. Res 1978, 65 (2), 163–172. DOI:10.1016/s002-5320(78)90053-9. [PubMed: 731784]
3. Goldberg M; Kulkarni AB; Young M; Boskey A, Dentin: structure, composition and mineralization. Front. Biosci 2011, 3, 711–35. DOI:10.2741/e281.
4. White SN; Paine ML; Luo W; Sarikaya M; Fong H; Yu Z; Li ZC; Snead ML, The dentino-enamel junction is a broad transitional zone uniting dissimilar bioceramic composites. J. Am. Ceram. Soc 2000, 83 (1), 238–40. DOI:10.1111/j.1151-2916.2000.tb01181.x.
5. Imbeni V; Kruzic J; Marshall G; Marshall S; Ritchie R, The dentin–enamel junction and the fracture of human teeth. Nat. Mater 2005, 4 (3), 229 DOI:10.1038/nmat1323. [PubMed: 15711554]
6. Jakupović S; Anić I; Ajanović M; Korać S; Konjhodžić A; Džanković A; Vuković A, Biomechanics of cervical tooth region and noncarious cervical lesions of different morphology; three-dimensional finite element analysis. Eur. J. Dent 2016, 10 (3), 413 DOI:10.4103/1305-7456.184166. [PubMed: 27403064]
7. Soares P; Machado A; Zeola L; Souza P; Galvão A; Montes T; Pereira A; Reis B; Coleman T; Grippo J, Loading and composite restoration assessment of various non-carious cervical lesions morphologies–3D finite element analysis. Aust. Dent. J 2015, 60 (3), 309–316. DOI:10.1111/adj.12233. [PubMed: 25312697]
8. Cao C; Mei M; Li Q.-l.; Lo E; Chu C, Methods for biomimetic mineralisation of human enamel: a systematic review. Materials 2015, 8 (6), 2873–2886. DOI: 10.3390/ma8062873.
9. Ruan Q; Moradian-Oldak J, Amelogenin and enamel biomimetics. J. Mater. Chem. B 2015, 3 (16), 3112–3129. DOI: 10.1039/c5tb00163c. [PubMed: 26251723]
10. Ruan Q; Zhang Y; Yang X; Nutt S; Moradian-Oldak J, An amelogenin–chitosan matrix promotes assembly of an enamel-like layer with a dense interface. Acta Biomater. 2013, 9 (7), 7289–7297. DOI: 10.1016/j.actbio.2013.04.004. [PubMed: 23571002]
11. Mukherjee K; Ruan Q; Liberman D; White SN; Moradian-Oldaka J, Repairing human tooth enamel with leucine-rich amelogenin peptide–chitosan hydrogel. J. Mater. Res 2016, 31(5), 556–563. DOI: 1557/JMR.2016.64.
12. Mukherjee K; Ruan QH; Nutt S; Tao JH; De Yoreo JJ; Moradian-Oldak J, Peptide-Based Bioinspired Approach to Regrowing Multilayered Aprismatic Enamel. Acs Omega 2018, 3 (3), 2546–2557. DOI:10.1021/acsomega.7b02004. [PubMed: 29623301]
13. Prajapati S; Ruan Q; Mukherjee K; Nutt S; Moradian-Oldak J, The Presence of MMP-20 Reinforces Biomimetic Enamel Regrowth. J. Dent. Res 2018, 97 (1), 84–90. DOI: 10.1177/0022034517728504. [PubMed: 28846464]
14. Mukherjee K; Ruan Q; Moradian-Oldak J, Peptide-Mediated Biomimetic Regrowth of Human Enamel In Situ In Odontogenesis, Springer: 2019; pp 129–138. DOI: 10.1007/978-1-4939-9012-2_13.
15. Klein OD; Duverger O; Shaw W; Lacruz RS; Joester D; Moradian-Oldak J; Pugach MK; Wright JT; Millar SE; Kulkarni AB, Meeting report: a hard look at the state of enamel research. Int. J. Oral Sci 2017, 9 (11), e3 DOI: 10.1038/ijos.2017.40. [PubMed: 29165423]
16. Pandya M; Diekwisch TG, Enamel biomimetics—fiction or future of dentistry. Int. J. Oral Sci 2019, 11(1), 8 DOI: 10.1038/s41368-018-0038-6. [PubMed: 30610185]
17. Niu L.-n.; Zhang W; Pashley DH; Breschi L; Mao J; Chen J.-h.; Tay FR, Biomimetic remineralization of dentin. Dent. Mater 2014, 30 (1), 77–96. DOI: 10.1016/j.dental.2013.07.013. [PubMed: 23927881]
18. Cao C; Mei M; Li Q-L; Lo E; Chu C, Methods for biomimetic remineralization of human dentine: a systematic review. Int. J. Mol. Sci 2015, 16 (3), 4615–4627. DOI: 10.3390/ijms16034615. [PubMed: 25739078]
19. Tay F; Pashley DH, Biomimetic remineralization of resin-bonded acid-etched dentin. J. Dent. Res 2009, (8), 719–724. DOI: 10.1177/0022034509341826. [PubMed: 19734458]

20. Beniash E; Simmer JP; Margolis HC, The effect of recombinant mouse amelogenins on the formation and organization of hydroxyapatite crystals in vitro. J. Struct. Biol 2005, 149 (2), 182–190. DOI:10.1016/j.jsb.2004.11.001. [PubMed: 15681234]
21. Fincham AG; Moradian-Oldak J; Simmer JP, The structural biology of the developing dental enamel matrix. J. Struct. Biol 1999, 126 (3), 270–299. DOI:10.1006/jsbi.1999.4130. [PubMed: 10441532]
22. Liang KN; Gao Y; Li JS; Liao Y; Xiao SM; Zhou XD; Li JY, Biomimetic mineralization of collagen fibrils induced by amine-terminated PAMAM dendrimers - PAMAM dendrimers for remineralization. J Biomat Sci-Polym E 2015, 26 (14), 963–974. DOI: 10.1080/09205063.2015.1068606.
23. Wright JT; Li Y; Suggs C; Kuehl MA; Kulkarni AB; Gibson CW, The role of amelogenin during enamel-crystallite growth and organization in vivo. Eur. J. Oral Sci 2011, 119, 65–69. DOI: 10.1111/j.1600-0722.2011.00883.x. [PubMed: 22243229]
24. Gibson CW; Yuan ZA; Hall B; Longenecker G; Chen EH; Thyagarajan T; Sreenath T; Wright JT; Decker S; Piddington R; Harrison G; Kulkarni AB, Amelogenin-deficient mice display an amelogenesis imperfecta phenotype. J. Biol. Chem 2001, 276 (34), 31871–31875. DOI: 10.1074/jbc.M104624200. [PubMed: 11406633]
25. Hu YY; Smith CE; Cai ZH; Donnelly LAJ; Yang J; Hu JCC; Simmer JP, Enamel ribbons, surface nodules, and octacalcium phosphate in C57BL/6 Amelx(−/−) mice and Amelx(+/−) lyonization. Mol. Genet. Genom. Med 2016, 4 (6), 641-+ DOI: 10.1002/mgg3.252.
26. Bidlack FB; Xia Y; Pugach MK, Dose-Dependent Rescue of KO Amelogenin Enamel by Transgenes in Vivo. Front. Physiol 2017, 8 DOI: Artn 932 10.3389/Fphys.2017.00932.
27. Jágr M; Ergang P; Pataridis S; Kolrosová M; Bartoš M; Mikšík I, Proteomic analysis of dentin–enamel junction and adjacent protein-containing enamel matrix layer of healthy human molar teeth. Eur. J. Oral Sci 2019, 127 (2), 112–121. DOI: 10.1111/eos.12594. [PubMed: 30466169]
28. Papagerakis P; MacDougall M; Hotton D; Bailleul-Forestier I; Oboeuf M; Berdal A, Expression of amelogenin in odontoblasts. Bone 2003, 32 (3), 228–240. DOI: 10.1016/S8756-3282(02)00978-X. [PubMed: 12667550]
29. Deshpande AS; Fang P-A; Simmer JP; Margolis HC; Beniash E, Amelogenin-collagen interactions regulate calcium phosphate mineralization in vitro. J. Biol. Chem 2010, 285(25), 19277–19287. DOI:10.1074/jbc.m109.079939. [PubMed: 20404336]
30. Nudelman F; Lausch AJ; Sommerdijk NAJM; Sone ED, In vitro models of collagen biomineralization. J. Struct. Biol 2013, 183 (2), 258–269. DOI: 10.1016/j.jsb.2013.04.003. [PubMed: 23597833]
31. Shen C; Zhang NZ; Anusavice KJ, Fluoride and Chlorhexidine Release from Filled Resins. J. Dent.Res 2010, 89 (9), 1002–1006. DOI: 10.1177/0022034510374055. [PubMed: 20581354]
32. Xu HHK; Moreau JL; Sun LM; Chow LC, Nanocomposite containing amorphous calcium phosphate nanoparticles for caries inhibition. Dent. Mater 2011, 27 (8), 762–769. DOI: 1016/j.dental.2011.03.016. [PubMed: 21514655]
33. Gandolfi MG; Taddei P; Siboni F; Modena E; De Stefano ED; Prati C, Biomimetic remineralization of human dentin using promising innovative calcium-silicate hybrid “smart” materials. Dent. Mater 2011, 27 (11), 1055–1069. DOI: 10.1016/j.dental.2011.07.007. [PubMed: 21840044]
34. Sauro S; Osorio R; Watson TF; Toledano M, Therapeutic effects of novel resin bonding systems containing bioactive glasses on mineral-depleted areas within the bonded-dentine interface. J. Mater. Sci-Mater. M 2012, 23 (6), 1521–1532. DOI: 10.1007/s10856-012-4606-6. [PubMed: 22466816]
35. Olszta MJ; Douglas EP; Gower LB, Intrafibrillar mineralization of collagen using a liquid-phase mineral precursor. Mater. Res. Soc. Symp. P 2003, 774, 127–134. DOI: 10.1074/jbc.m109.079939.
36. Saxena N; Cremer MA; Dolling ES; Nurrohman H; Habelitz S; Marshall GW; Gower LB, Influence of fluoride on the mineralization of collagen via the polymer-induced liquid-precursor (PILP) process. Dent. Mater 2018, 34 (9), 1378–1390. DOI: 10.1016/j.dental.2018.06.020. [PubMed: 29935767]

37. Gu L; Kim YK; Liu Y; Ryou H; Wimmer CE; Dai L; Arola DD; Looney SW; Pashley DH; Tay FR, Biomimetic Analogs for Collagen Biomineralization. J. Dent. Res 2011, 90 (1), 82–87. DOI:1177/0022034510385241. [PubMed: 20940362]
38. Sun J; Chen CQ; Pan HH; Chen Y; Mao CY; Wang W; Tang RK; Gu XH, Biomimetic promotion of dentin remineralization using L-glutamic acid: inspiration from biomineralization proteins. J. Mater. Chem. B 2014, 2 (28), 4544–4553. DOI: 10.1039/c4tb00451e. [PubMed: 32261555]
39. Wang Q; Wang XM; Tian LL; Cheng ZJ; Cui FZ, In situ remineralizaiton of partially demineralized human dentine mediated by a biomimetic non-collagen peptide. Soft Matter 2011, 7 (20), 9673–9680. DOI:10.1039/c1sm05018d.
40. Niu LN; Jee SE; Jiao K; Tonggu L; Li M; Wang L; Yang YD; Bian JH; Breschi L; Jang SS; Chen JH; Pashley DH; Tay FR, Collagen intrafibrillar mineralization as a result of the balance between osmotic equilibrium and electroneutrality. Nat. Mater 2017, 16 (3), 370–378. DOI: 10.1038/NMAT4789. [PubMed: 27820813]
41. Han M; Li QL; Cao Y; Fang H; Xia R; Zhang ZH, In vivo remineralization of dentin using an agarose hydrogel biomimetic mineralization system. Sci. Rep 2017, 7 DOI: Artn 4195510.1038/Srep41955.
42. Ning TY; Xu XH; Zhu LF; Zhu XP; Chu CH; Liu LK; Li QL, Biomimetic mineralization of dentin induced by agarose gel loaded with calcium phosphate. J. Biomed. Mater. Res. B 2012, 100B (1), 138–144. DOI:10.1002/jbm.b.31931.
43. Li JH; Yang JJ; Li JY; Chen L; Liang KN; Wu W; Chen XY; Li JS, Bioinspired intrafibrillar mineralization of human dentine by PAMAM dendrimer. Biomaterials 2013, 34 (28), 6738–6747. DOI: 1016/j.biomaterials.2013.05.046. [PubMed: 23787113]
44. Deshpande AS; Beniash E, Bio-inspired Synthesis of Mineralized Collagen Fibrils. Cryst. Growth Des 2008, 8 (8), 3084–3090. DOI: 10.1021/cg800252f.
45. Vermeer LS, Marquette A, Schoup M, Fenard D, Galy A, Bechinger B, Simultaneous analysis of secondary structure and light scattering from circular dichroism titrations: application to vectofusin-1, Sci. Rep 2016, 6 39450. [PubMed: 28004740]
46. Schmid TM; Linsenmayer TF, Denaturation-renaturation properties of two molecular forms of short-chain cartilage collagen. Biochemistry-Us 1984, 23 (3), 553–558. DOI: 10.1021/bi00298a024.
47. Liu Y; Kim YK; Dai L; Li N; Khan SO; Pashley DH; Tay FR, Hierarchical and non-hierarchical mineralisation of collagen. Biomaterials 2011, 32 (5), 1291–1300. DOI: 10.1016/j.biomaterials.2010.10.018. [PubMed: 21040969]
48. Legeros RZ, Apatites in Biological-Systems. Prog. Cryst. Growth Ch 1981, 4 (1–2), 1–45. DOI:10.1016/0146-3535(81)90046-0.
49. Nishitani Y; Yoshiyama M; Tay F; Wadgaonkar B; Waller J; Agee K; Pashley DH, Tensile strength of mineralized/demineralized human normal and carious dentin. J. Dent. Res 2005, 84 (11), 1075–1078. DOI:10.1177/154405910508401121. [PubMed: 16246945]
50. Hu JCC; Hu YY; Lu YH; Smith CE; Lertlam R; Wright JT; Suggs C; McKee MD; Beniash E; Kabir ME; Simmer JP, Enamelin Is Critical for Ameloblast Integrity and Enamel Ultrastructure Formation. Plos One 2014, 9 (3). DOI: ARTNe8930310.1371/journal.pone.0089303.
51. Kim JW; Nam SH; Jang KT; Lee SH; Kim CC; Hahn SH; Hu JCC; Simmer JP, A novel splice acceptor mutation in the DSPP gene causing dentinogenesis imperfecta type II. Hum. Genet 2004, 115 (3), 248–254. DOI: 10.1007/s00439-004-1143-5. [PubMed: 15241678]
52. Colfen H, Biomineralization a Crystal-Clear View. Nat. Mater 2010, 9 (12), 960–961. DOI:38/nmat2911. [PubMed: 21102512]
53. Toroian D; Lim JE; Price PA, The size exclusion characteristics of type I collagen - Implications for the role of noncollagenous bone constituents in mineralization. J. Biol. Chem 2007, 282 (31), 22437–22447. DOI: 10.1074/jbc.M700591200. [PubMed: 17562713]
54. Mazzoni A; Tjäderhane L; Checchi V; Di Lenarda R; Salo T; Tay F; Pashley DH; Breschi L, Role of dentin MMPs in caries progression and bond stability. J. Dent. Res 2015, 94 (2), 241–251. DOI:10.1177/0022034514562833. [PubMed: 25535202]

55. Jiao K; Niu LN; Ma CF; Huang XQ; Pei DD; Luo T; Huang Q; Chen JH; Tay FR, Complementarity and Uncertainty in Intrafibrillar Mineralization of Collagen. Adv. Funct. Mater 2016, 26 (38), 6858–6875. DOI: 10.1002/adfm.201602207.

56. Wang Y; Azais T; Robin M; Vallee A; Catania C; Legriel P; Pehau-Arnaudet G; Babonneau F; Giraud-Guille MM; Nassif N, The predominant role of collagen in the nucleation, growth, structure and orientation of bone apatite. Nat. Mater 2012, 11 (8), 724–733. DOI: 10.1038/NMAT3362. [PubMed: 22751179]

57. Moradian-Oldak J; Bouropoulos N; Wang LL; Gharakhanian N, Analysis of self-assembly and apatite binding properties of amelogenin proteins lacking the hydrophilic C-terminal. Matrix Biol. 2002, 21 (2), 197–205 DOI: 10.1016/S0945-053x(01)00190-1. [PubMed: 11852235]

58. Vidal C; Tjäderhane L; Scaffa P; Tersariol I; Pashley D; Nader H; Nascimento F; Carrilho M, Abundance of MMPs and cysteine cathepsins in caries-affected dentin. J Dent Res 2014, 93 (3), 269–274. DOI:10.1177/0022034513516979. [PubMed: 24356440]

59. George A; Veis A, Phosphorylated Proteins and Control over Apatite Nucleation, Crystal Growth, and Inhibition. Chem. Rev 2008, 108 (11), 4670–4693. DOI: 10.1021/cr0782729. [PubMed: 18831570]

60. Forien J-B; Fleck C; Cloetens P; Duda G; Fratzl P; Zolotoyabko E; Zaslansky P, Compressive residual strains in mineral nanoparticles as a possible origin of enhanced crack resistance in human tooth dentin. Nano letters 2015, 15 (6), 3729–3734. DOI: 10.1021/acs.nanolett.5b00143. [PubMed: 26009930]

61. Kinney JH; Habelitz S; Marshall SJ; Marshall GW, The importance of intrafibrillar mineralization of collagen on the mechanical properties of dentin. J. Dent. Res 2003, 82 (12), 957–961. DOI:1177/154405910308201204. [PubMed: 14630894]

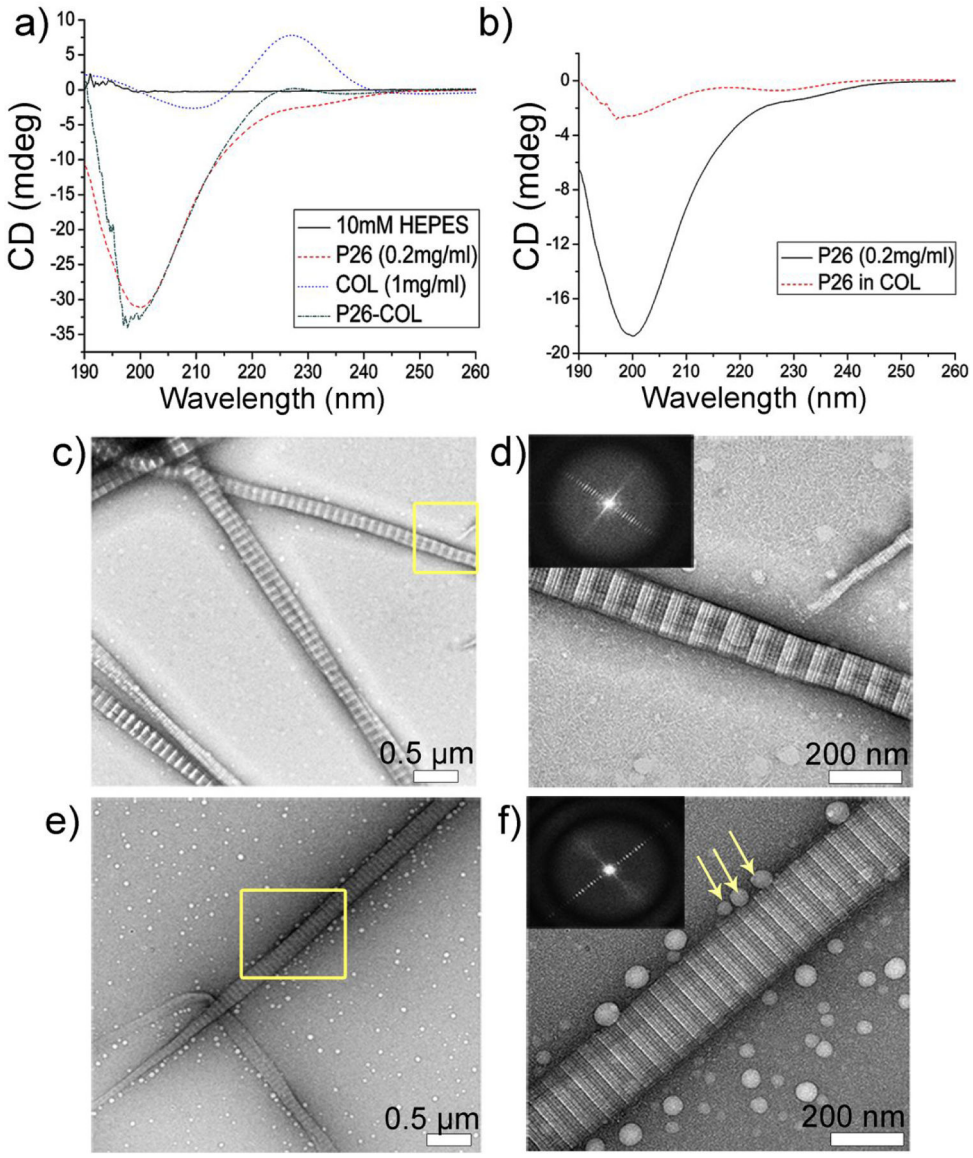

Figure 1.

Collagen-P26 interaction and assembly. (a) Circular dichroism (CD) spectra of collagen, P26 and collagen/P26 mixture after incubation at 25 C and at pH 7.15. (b) The normalized secondary structural changes in P26 after mixing with collagen compared to P26 alone. (c) and (d) Negatively stained TEM images of collagen self-assembly to fibrils in PBS after incubation at 25 C for 2 h at low and high magnification respectively. (e) and (f) Negatively stained TEM images of P26-collagen self-assembly in PBS after incubation at 25 C for 2 h at low and high magnification respectively. The insets in d and f are the Fourier Transform data showing the *d*-spacing of collagen fibrils (~67 nm). Peptide P26 assembly can be seen as dispersed nanospheres aligned closely along the collagen fibril (yellow arrows in f).

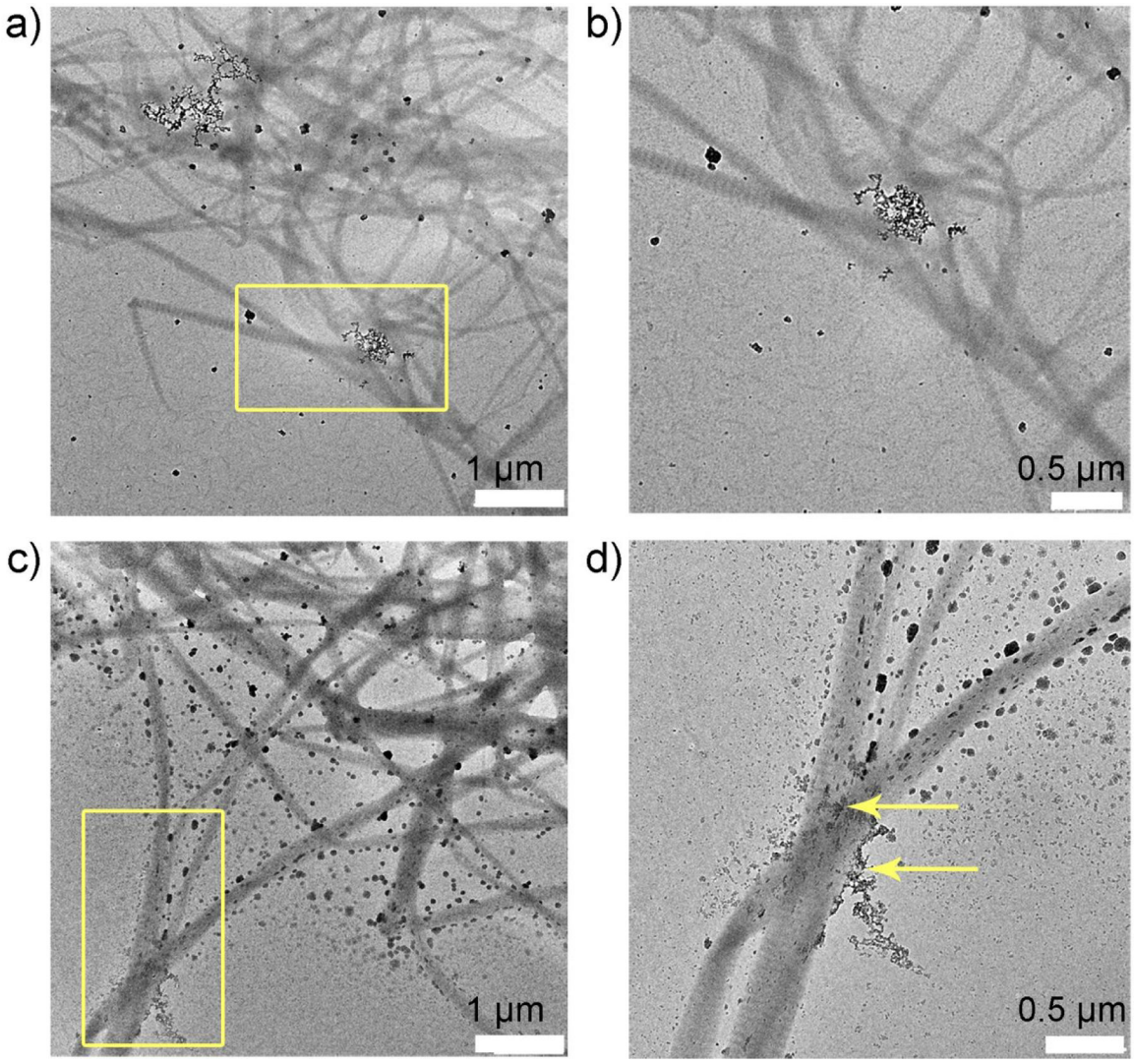

Figure 2.

Collagen-P26 mineralization after 1 hour. Unstained TEM images of collagen mineralization *in vitro* for 1 h in the control sample (no P26) at (a) low and its corresponding (b) high resolution of yellow square in (a). There are very few amorphous particles seen on the grid surface. TEM images of collagen mineralization *in vitro* for 1 h in the presence of P26 at (c) low and its corresponding (d) high resolution of yellow square in (c). Some of the fibrils in grid space (d) appear swollen with the precipitation of amorphous minerals on the surface (yellow arrows).

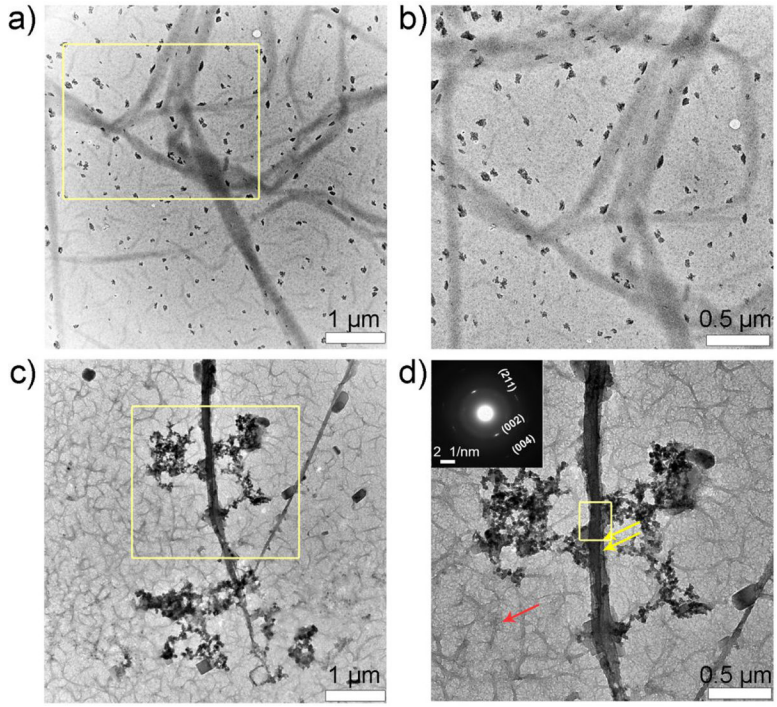

Figure 3.

Collagen-P26 mineralization after 2.5 hours. Unstained TEM images of collagen mineralization *in vitro* for 2.5 h in the control sample (no P26) at (a) low and its corresponding (b) high resolution of yellow square in (a). There are randomly scattered larger-sized mineral aggregates seen on the grid surface. TEM images of collagen mineralization *in vitro* for 2.5 h in the presence of P26 at (c) low and its corresponding (d) high resolution of yellow square in (c). Electron-dense fibrils can be seen on the grid surface along with formation of mineral deposits (yellow arrows in d). Selected-area electron diffraction data of fibril taken from (d) in inset indicates the presence of mature apatite crystals on collagen fibril. Yellow box in (d) indicates the area where SAED was recorded.

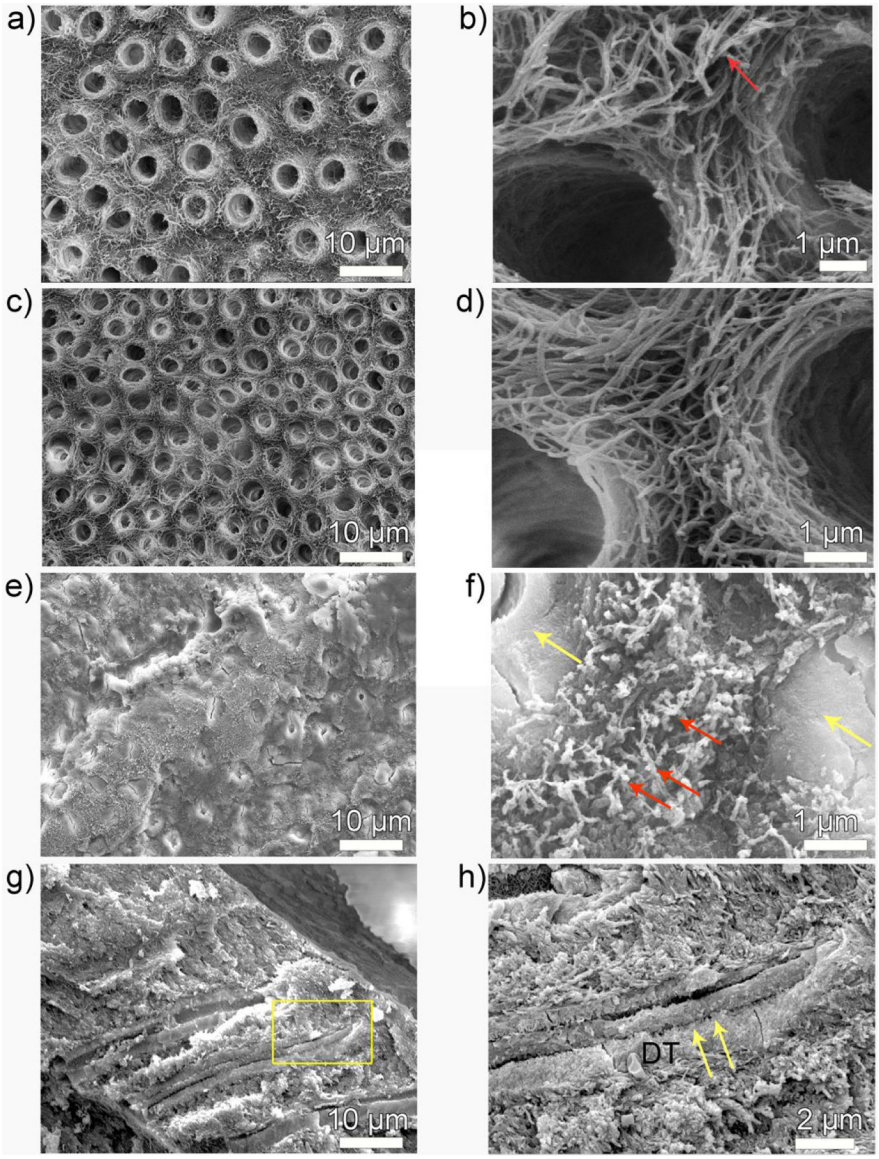

Figure 4.

SEM images of demineralized dentin surface before and after remineralization. (a, b) 3-day demineralized dentin, (c, d) control and (e-h) P26-treated dentin discs after incubation in artificial saliva in pH 7.0 at 37 °C. Images (b, d, f, h) are the high resolution corresponding magnified images of (a, c, e and g) respectively. (b) is a high-resolution SEM image of demineralized, mineral-depleted, collagen fibrils of intertubular dentin, giving a smooth ribbon-like appearance (red arrow). (c, d) There is no HAP crystallization on the surface of dentin in the control dentin discs and the tubules remain open. (e, f). After P26 application, the surface of dentinal tubule is completely occluded by a dense layer of HAP mineral precipitate (yellow arrows) and the exposed collagen fibrils are embedded in electron-dense mineralized areas (red arrows in f). (g, h) Cross-sections of the dentin discs show penetration of mineral ions up to 15 μm into the subsurface adhering firmly to the walls of the dentinal tubules (yellow arrows). *DT- dentinal tubule*.

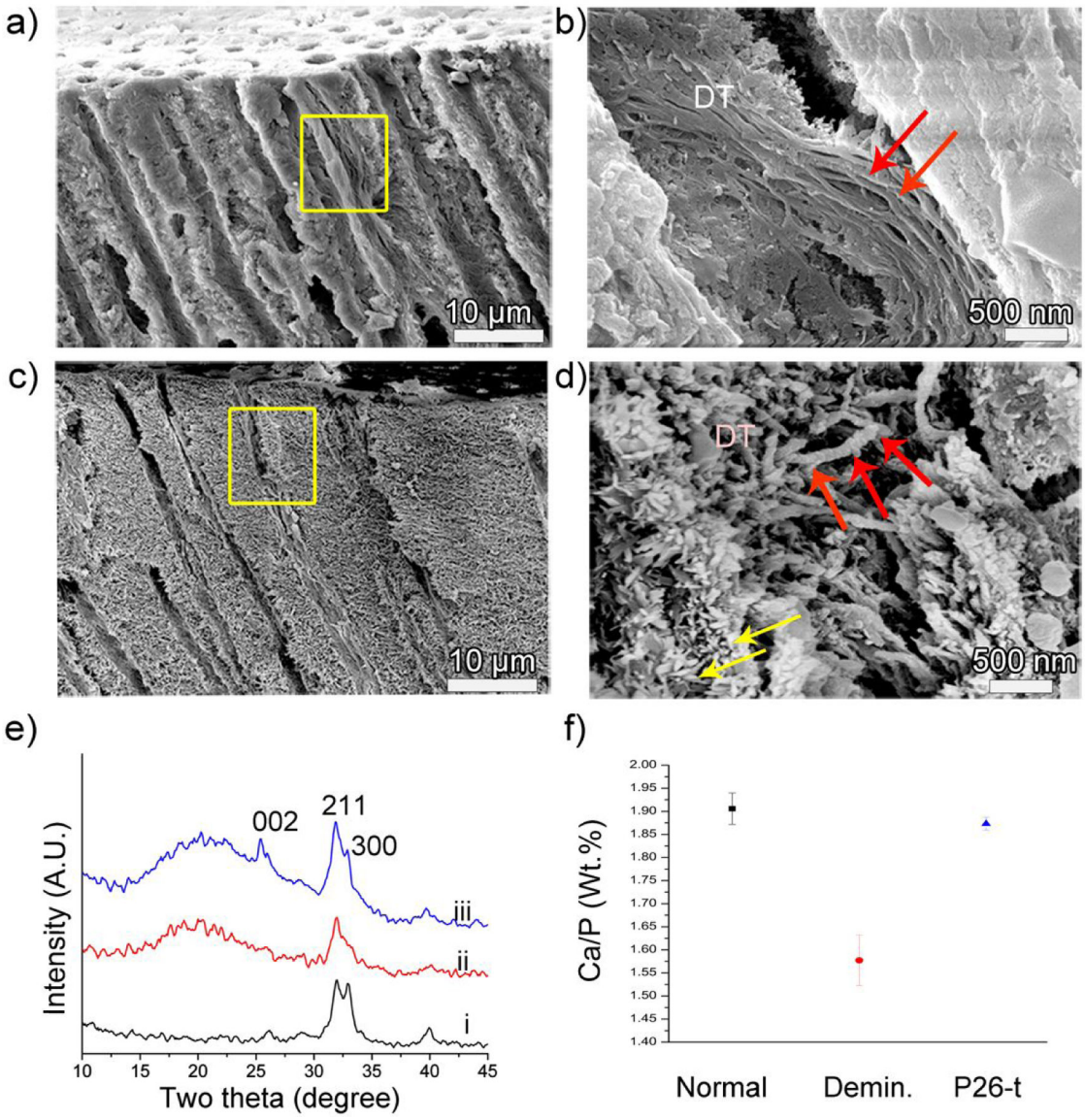

Figure 5.

Cross-sectional SEM images of dentin after remineralization. (a, b) control and (c, d) P26-treated dentin discs after 10 days of incubation in artificial saliva in pH 7.0 at 37 °C. Images (b, d) are the corresponding magnified images showing a single dentinal tubule of (a, c) in the yellow squares respectively. Figure (b) depicts the lack of mineralization of collagen fibers inside a dentinal tubule in the control. (d) After P26 application there is a marked depth of mineral deposition inside the tubule up to 15 μm from the surface. Newly formed crystals can be seen growing along the walls of the tubules (yellow arrows) and the diameter of the individual collagen fibers increases with time, giving a ‘beaded string-like’ appearance due to HAP precipitation (red arrows). (e) XRD spectra of (i) sound dentin, (ii) demineralized and (iii) remineralized dentin surfaces after P26 application. Distinct peaks for peptide-treated dentin discs indicate improved crystallinity of HAP when compared to ii.

(f) EDX data showing Ca/P weight ratio (weight %) on the surfaces of healthy, demineralized and P26-treated dentin *(n=3)*.

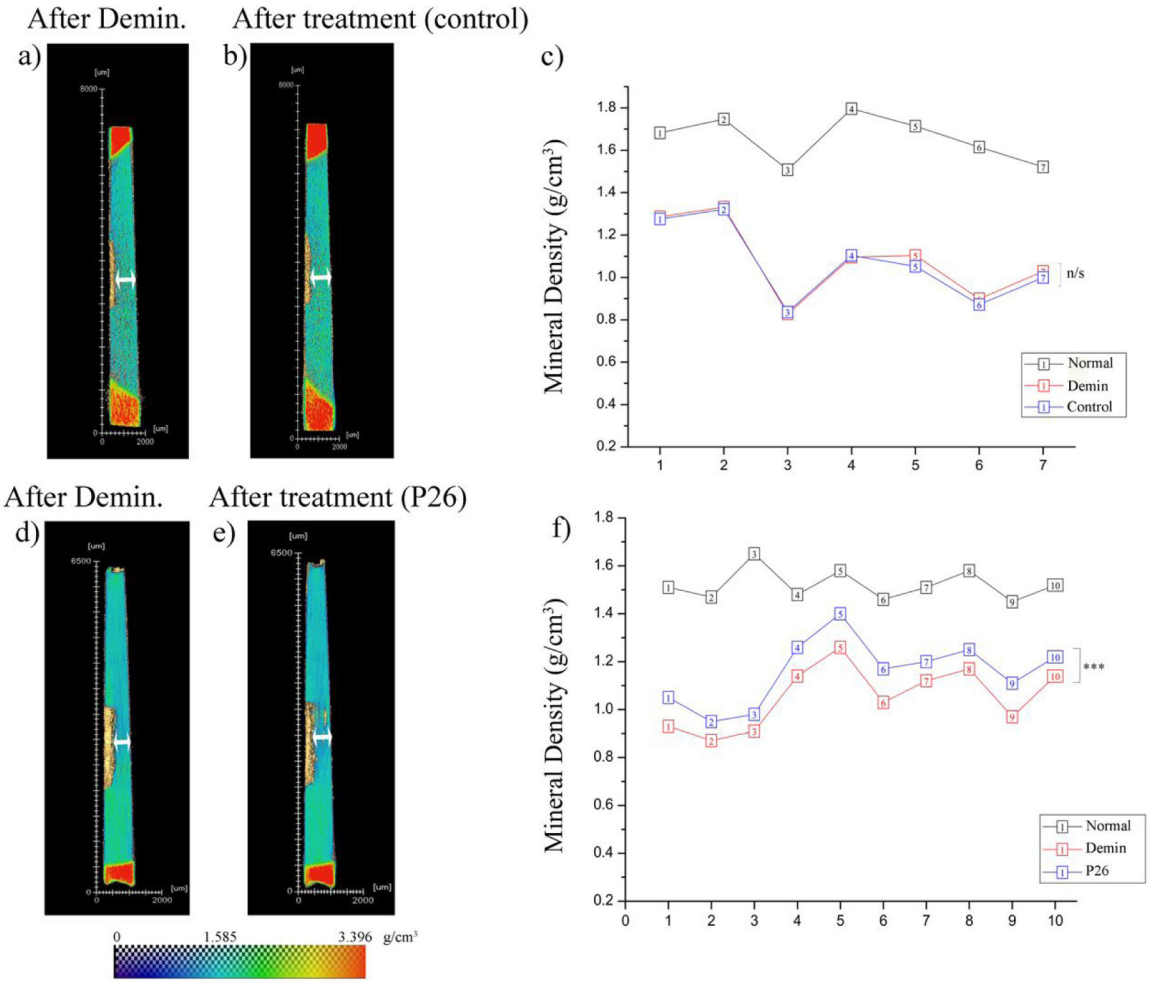

Figure 6.

Micro-CT analysis of demineralized dentin before and after remineralization. Heatmap images of transverse dentin discs showing (a) demineralized and (b) control dentin (turquoise), surrounded by tooth enamel at ends (red). Experimentally obtained MD values of sound enamel and dentin were used for calibration of heatmap color scale. There is no discernible change in lesion depth in the control sample following 10 days of incubation in artificial saliva. (c) Individual data points representing MD (mineral density) sample wise for normal, demineralized and control dentin (n=7). There is no change in MD between the demineralized and control groups. (d, e) Heatmap images of transverse dentin discs showing (d) demineralized and P26-treated dentin. There is a visible decrease in lesion depth in the peptide treated sample following 10 days of incubation in artificial saliva. (f) Individual data points representing MD values sample wise for normal, demineralized and P26-treated dentin (n=10). The gain in MD after peptide application is statistically significant (p < 0.001). Note: (n/s: non-significant difference).

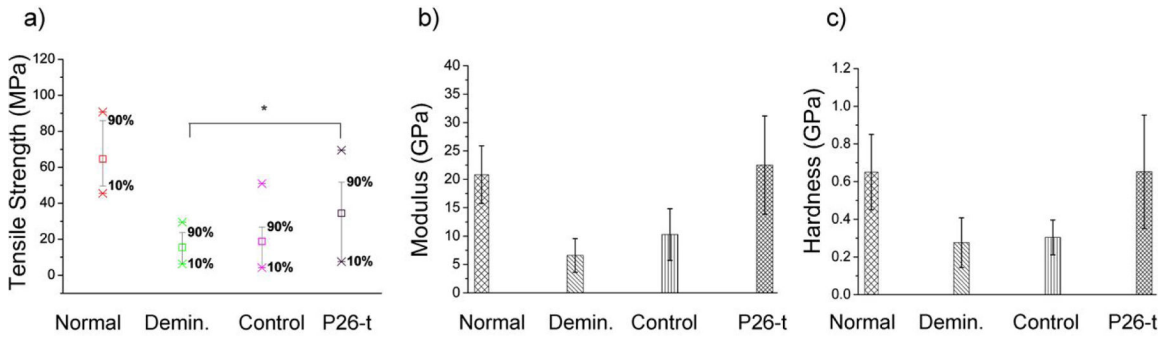

Figure 7.

Mechanical Properties of remineralized dentin. (a) Mean tensile strength (TS) of normal (n=15), demineralized (n=10), control (n=10) and P26-treated (n=10) dentin samples. The increase in the TS of dentin samples after P26 application is statistically significant ($p < 0.05$). The whiskers were drawn down to the 10th percentile and up to the 90th. Points below and above the whiskers were drawn as individual points. Nanoindentation tests showing mean (b) elastic modulus and (c) nano-hardness of the intact dentin, demineralized dentin, and the samples with (P26-treated) and without (control) after 10 days of remineralization (n =3 per group). Student's t-test was applied to identify differences in the hardness and elastic modulus between demineralized and repaired dentin ($p < 0.05$).